Materials Characterization 169 (2020) 110569

Contents lists available at ScienceDirect

Materials Characterization

journal homepage: www.elsevier.com/locate/matchar

Creep induced precipitation of the $(Cr,Mo)_5B_3$-type boride in γ/γ′ eutectic of a Ni-based superalloy

Hualong Ge[a,b], Yaqian Yang[c], Shijian Zheng[a,d,*], Kui Liu[c], Xiuliang Ma[a]

[a] Shenyang National Laboratory for Materials Science, Institute of Metal Research, Chinese Academy of Sciences, 110016 Shenyang, China
[b] School of Materials Science and Engineering, University of Science and Technology of China, 230026 Hefei, China
[c] Institute of Metal Research, Chinese Academy of Sciences, 110016 Shenyang, China
[d] Tianjin Key Laboratory of Materials Laminating Fabrication and Interface Control Technology, School of Materials Science and Engineering, Hebei University of Technology, Tianjin 300130, China

ARTICLE INFO

Keywords:
Ni-based superalloy
Transmission electron microscopy
Boride
Eutectic

ABSTRACT

Boron segregation and boride formation at grain boundaries are generally accepted in Ni-based superalloys. However, the addition of boron was found to result in the formation of a high density of nanosized M_5B_3 (where M is a mixture of Cr, Mo) particles in γ/γ′ eutectics of a Ni-based superalloy during high-temperature creep in this work. M_5B_3 phase precipitated at γ/γ′ eutectics keeps a well-defined orientation relationship with the eutectics, which is $[001]_{\gamma/\gamma'}//[001]_{M5B3}$, $(020)_{\gamma/\gamma'}//(130)_{M5B3}$. And these nanosized borides could block dislocation slip, result in stress concentration surrounding γ/γ′ eutectics and facilitate crack initiation at γ/γ′ eutectic/matrix interface during the creep at high temperatures.

1. Introduction

Ni-based superalloys have been widely used in aero-engines and industrial gas turbines due to their excellent high-temperature mechanical properties [1]. To achieve the long-term goal of developing new high-temperature propulsion materials to meet the capability needs of new jet engines, multi-disciplinary basic and applied researches such as influence mechanism of secondary phases are urgently required [2–5]. One of the objectives of basic research is to explore the high-temperature mechanism of the effects of minor elements such as boron. In polycrystalline superalloys, boron, as well as carbon, is usually added to enhance grain boundary strength at high temperatures and therefore improve creep strength and ductility [6]. Generally, it is accepted that boron usually segregates or forms borides at grain boundaries [7–12]. For instance, P. Kontis et al. [13,14] reported that boron could lead to serration of the grain boundaries retarding void formation and cavity propagation along grain boundaries, so as to improve the ductility. Meanwhile, the addition of boron is considered particularly to lower the incipient melting point of alloys [15] and facilitate eutectics formation, such as γ/γ′ eutectic [16]. As one of the most inhomogeneous microstructure components, γ/γ′ eutectics can form in most superalloys, including Ni-based [17] and Ni_3Al-based [18] superalloys, and the effect of γ/γ′ eutectics on the mechanical properties of superalloys cannot be ignored.

Previous investigations showed that excessive or misoriented eutectic usually leads to a deterioration in mechanical properties at elevated temperatures [16,19]. It was found that γ/γ′ eutectic can nucleate heterogeneously and grow on MC-type carbide in Ni-based single crystal superalloys [20]. The γ/γ′ eutectics can inherit the orientation of MC and present misorientation with the eutectic-free γ/γ′ matrix, leading to a decrease of mechanical properties of superalloys. Moreover, observation by Zhang et al. [21] has found that fine borides could precipitate in γ/γ′ eutectics in M91 alloy after prolonged aging at 850 °C, which indicates that a higher content of boron in γ/γ′ eutectics than that of primary γ/γ′ matrix exists. The low solubility of boron and higher boron content will result in a strong tendency for boride precipitation in γ/γ′ eutectics region. Since the γ/γ′ eutectics was believed to decrease ductility by cleavage fracture or providing sites for cracks initiation at γ/γ′ eutectics/matrix interface [17,22], the boride precipitation in γ/γ′ eutectics will inevitably further affect the mechanical behavior. There were many researchers who reported the precipitation of borides in superalloys [13,14,23,24], but most of them focused on the precipitation along grain boundaries. As borides could precipitate in γ/γ′ eutectics during long-term aging, accordingly it is understandable

* Corresponding author at: Tianjin Key Laboratory of Materials Laminating Fabrication and Interface Control Technology, School of Materials Science and Engineering, Hebei University of Technology, Tianjin 300130, China.
E-mail addresses: gehualong@csu.edu.cn (H. Ge), yangyq@imr.ac.cn (Y. Yang), sjzheng@hebut.edu.cn (S. Zheng), kliu@imr.ac.cn (K. Liu), xlma@imr.ac.cn (X. Ma).

https://doi.org/10.1016/j.matchar.2020.110569
Received 8 July 2020; Received in revised form 12 August 2020; Accepted 13 August 2020
Available online 17 August 2020
1044-5803/

Table 1
Chemical composition of the alloy in this work (wt%).

B	C	Co	Cr	Mo	Al	Ti	V	Zr	Ni
0.023	0.16	9.65	9.19	3.02	5.20	4.32	0.71	0.086	Bal.

that creep can promote the boride precipitation in γ/γ′ eutectics. Nevertheless, more detailed investigations on the microstructural evolution of γ/γ′ eutectics are necessary to understand the role of microstructure during creep at high temperatures.

The primary object of the present work is, therefore, employing advanced transmission electron microscopy (TEM), to clarify more detail microstructure characteristics of γ/γ′ eutectics of a crept Ni-based superalloy. It has been found that an amount of granular M_5B_3 phase precipitated in γ/γ′ eutectics. This work is helpful to understand the role of γ/γ′ eutectic microstructure in the creep process of superalloys.

2. Materials and methods

The alloy investigated in this work was a K417G alloy, and the nominal chemical composition is given in Table 1. The master alloy was produced in an industrial scale vacuum induction furnace, following remelting and casting into bars. According to the requirements of standard GB/T 2039-2012 [25], as-cast specimens were machined to constant load stress rupture samples with a gauge diameter of 5 mm and a gauge length of 25 mm. The average grain size is about 2.5 mm (see Supplementary Material). Stress rupture tests were performed under the condition of 950 °C/235 MPa. The creep rupture life and elongation of creep specimens are about 45.45 h and 9.12%, respectively. After stress rupture tests, specimens were sectioned parallel to the stress axial line. Metallographic specimens were prepared via mechanical polishing and chemically etching in a solution with 5 g $CuSO_4$, 25 ml HCl and 40 ml H_2O. TEM thin foils were prepared by mechanical thinning and Ar ion milling method (Gatan precision ion polishing system (PIPS II)).

Macromorphological characterization and Electron probe microanalysis (EPMA) were performed on an electron probe micro-analyzer (Jeol JXA-8530F). Scanning transmission electron microscopy (STEM) imaging and Electron energy loss spectroscopy (EELS) analysis were performed on a Titan Cube 60-300, operated at 300 kV, equipped with a high-angle annular dark-field (HAADF) detector and a Gatan Quantum electron energy loss spectrometer. High-resolution TEM (HRTEM) imaging, selected-area electron diffraction (SAED) and chemical analysis were undertaken on an FEI Tecnai G^2 F30 microscope operating at 300 kV, equipped with an energy-dispersive spectrometer (EDS) system. Before loading into the TEM, the thin foils were cleaned by a Gatan 950 plasma system for removing surface contamination.

3. Results and discussion

Fig. 1(a) and (b) display the macrostructural features of γ/γ′ eutectics in as-cast and crept samples, respectively. The γ/γ′ eutectic zone can be separated into fine γ/γ′ area and coarse γ′ area according to the morphology feature of γ′ phases. Some blocky MC carbides displaying dark contrast in backscattered electron (BSE) mode are observed in these images. Interestingly, some particles displaying dark-grey contrast exist in the eutectic area of the crept sample, which may hint that fine secondary phases precipitated during high temperature creep. The change is evident from the locally magnified image of the framed area inserted in the top-right of Fig. 1(b). And so it is proved that excessive amounts of granular precipitates showing higher contrast than γ and γ′ phases formed in the γ channel in γ/γ′ eutectic zone in Fig. 1(c). A HAADF image (Fig. 1(d)) under higher magnification shows the morphology features of the precipitates. These nanosized precipitates about dozens of nanometers in size primarily located at γ/γ′ interface in eutectics. To display relative compositional distribution, EDS mapping analyses of the frame region in Fig. 1(d) were performed. Fig. 1(e)–(n) exhibit the alloying element segregation mappings. Higher B, C, V, Zr, Cr and Mo contents were found in the precipitates in comparison to those in γ/γ′ eutectic. This suggested that these fine secondary phase precipitates are possibly corresponding to carbides or borides. According to the EDS profile (in Fig. 1(o)), these fine secondary phase precipitates are mainly composed of B, Cr, Mo and a small amount of V, Co, Zr and Ni. The EELS technique, which is more sensitive to light elements, was used to confirm the presence of boron in the secondary phases. EELS result (in Fig. 1(p)) shows that the secondary phase really contains boron and chromium primarily.

From a viewpoint of thermodynamics, possible phases of the precipitates are Cr-based carbides and borides which contain similar elements in Ni-based superalloys. To identify the precipitates, electron diffraction analyses were performed. A HAADF image (in Fig. 2(a)) displays that the precipitate is actually at the γ/γ′ interface in eutectic. And the corresponding SAED patterns along $[001]_{\gamma/\gamma'}$ and $[\bar{1}01]_{\gamma/\gamma'}$ direction obtained from the region including both the precipitate and γ/γ′ in Fig. 2(a) are shown in Fig. 2(b) and (c), respectively. Based on the reflections from the precipitate, it can be identified that the precipitate has M_5B_3- type structure (space group I4/mcm) with lattice parameters $a = 5.64$ Å, $c = 10.72$ Å. The lattice parameter of γ/γ′ eutectic is about 3.62 Å. Moreover, the precipitate presents a good orientation relationship with γ/γ′ eutectic, which can be indexed as $[001]_{\gamma/\gamma'}//[130]_{M5B3}$, with $(200)_{\gamma/\gamma'}//(3\bar{1}0)_{M5B3}$, $(020)_{\gamma/\gamma'}//(006)_{M5B3}$.

In addition to orientation relationship $[001]_{\gamma/\gamma'}//[130]_{M5B3}$, $(200)_{\gamma/\gamma'}//(3\bar{1}0)_{M5B3}$, borides maintaining $[001]_{\gamma/\gamma'}//[001]_{M5B3}$, $(020)_{\gamma/\gamma'}//(130)_{M5B3}$ was also discovered in our alloy. As shown in the lower part of Fig. 2(d), the orientation relationship between M_5B_3 phase and γ/γ′ eutectic is $[001]_{\gamma/\gamma'}//[001]_{M5B3}$, $(020)_{\gamma/\gamma'}//(130)_{M5B3}$. Also it is interesting that M_5B_3 phase at the top of Fig. 2(d) exhibits an orientation relationship $[001]_{\gamma/\gamma'}//[130]_{M5B3}$, $(200)_{\gamma/\gamma'}//(3\bar{1}0)_{M5B3}$. Du et al. [26] reported that intergrowth of M_5B_3 phases with different crystal orientations at grain boundaries in IN792 alloy. The results here indicate this type of intergrowth also exists in the γ/γ′ eutectic zone in superalloys. A higher magnified image of the intergrowth zone shown in Fig. 2(e) displays an unobvious interface with $(310)_{M5B3}//(130)_{M5B3}$. For I4/mcm structure, $(310)_{M5B3}$ is equivalent to $(130)_{M5B3}$ in M_5B_3 phase. Actually, the two orientation relationships outlined above are equivalent, since $[001]_{\gamma/\gamma'}//[001]_{M5B3}$, $(020)_{\gamma/\gamma'}//(130)_{M5B3}$ can also be indexed as $[010]_{\gamma/\gamma'}//[130]_{M5B3}$, $(002)_{\gamma/\gamma'}//(006)_{M5B3}$. Though the mechanism of the intergrowth is still unclear at present, Du et al. [26] have proposed that two parts of the intergrown M_5B_3 phase may be formed by nucleation individually and grown up together, or one nucleation on another part. However, during our extensive TEM observations at γ/γ′ eutectic regions of crept samples, there is no evidence to prove that one nucleation on another part with different orientation exists in γ/γ′ eutectics. The initial M_5B_3 particles (less than 20 nm in size) we observed all nucleate individually.

It should be noted that, the precipitates in Fig. 1(c) displays a bright contrast, whereas in Fig. 1(d) the precipitates show a dark contrast. Generally speaking, HAADF images are termed *Z*-contrast images, but the HAADF detector usually can collect some Bragg electrons, leading to diffraction contrast in HAADF images. And Bragg effects can be avoided by decreasing the camera length and tilting the specimen to a major zone axis [27]. When Bragg effects are avoided, the precipitates will show a darker contrast in HAADF images (see Supplementary Material), which is consistent with the BSE image (Fig. 1(b)). And this issue also could be confirmed by HRTEM images shown in Fig. 3. Based on the (hk0) reflections present for $h + k = 2n$ in the Fast Fourier Transformed (FFT) pattern (inset in Fig. 3(a)), the precipitates showing bright contrast in Fig. 1(c) can be determined to be also M_5B_3 phase.

Moreover, by comparison with the γ/γ′ eutectics of crept specimens (Fig. 4(a)), no granular M_5B_3 precipitates exist in the γ/γ′ eutectics of as-cast specimens (Fig. 4(b)). And we annealed an as-cast sample for the same time and temperature of creep test. Though the nanosized M_5B_3

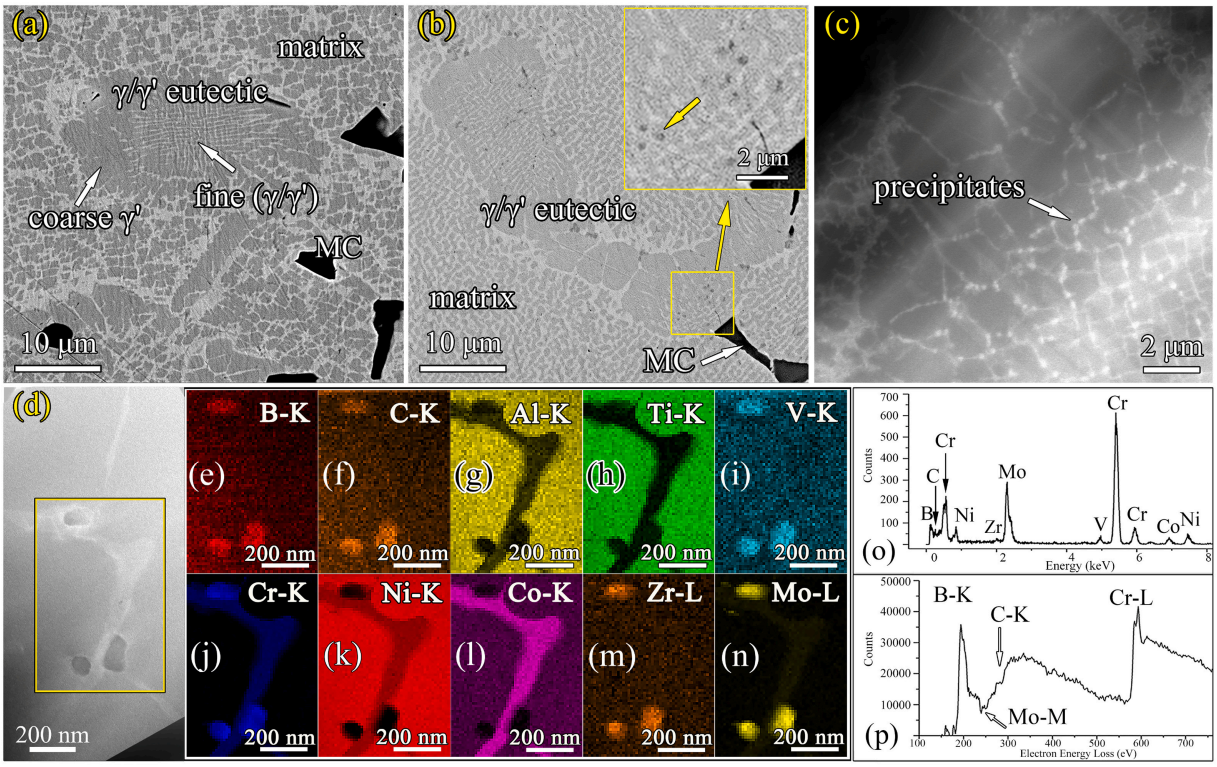

Fig. 1. The BSE micrographs showing the morphological features of γ/γ′ eutectics in (a) the as-cast and (b) the crept samples, and a locally magnified image of the frame in (b) showing that some dark-grey particles precipitated at γ/γ′ eutectic regions. A HAADF image showing a large number of nanosized precipitates in γ/γ′ eutectic zone in (c) and a HAADF image under higher magnification showing the precipitates in γ/γ′ in (d). (e–n) Displaying the related EDS mapping results; (o and p) showing the typical EDS spectrum and background subtracted EELS spectrum of these nanosized precipitates, respectively.

phase can precipitate in long-term aging Ni-based superalloys [28], no obvious precipitation was observed in the γ/γ′ eutectics of specimens annealed under the condition of 950 °C/45.45 h (see Fig. 4(c)). That is, the nanosized M_5B_3 borides formed during creep and this is not because of annealing. Thus, it is suggested that creep deformation promotes M_5B_3 phase formation.

While M_5B_3 usually precipitates at grain boundary in superalloys, precipitation of M_5B_3 boride in γ/γ′ eutectic during creep is an interesting finding. As shown in Fig. 4(d), M_5B_3 phase particles linked dislocations were observed in γ/γ′ eutectics. Segregation of Cr, Mo and Co at stacking faults and dislocations have been found in superalloys [29,30], and that was also confirmed by EDS line-scan profiles (Fig. 4(e)) in our alloy, whereas boron segregation at crystal defects have not been confirmed until now. Zhang et al. [31] suggested that crystal defects like dislocation can cause boron segregation, which provides the condition of boride nucleation during transient liquid phase bonding process. But it has not been experimentally validated. On the other hand, as the limited solubility of Cr, Mo in γ′ phase and the strong positive segregation tendency of boron, these elements will be enriched in the residual liquid during γ/γ′ eutectic reaction [15]. And Cr was found indeed to be enriched at the crown of γ/γ′ eutectics (see Fig. 4(f)). Since boron can promote γ/γ′ eutectic formation [15,32], it is reasonable to suspect that γ/γ′ eutectic contains a high concentration of boron. Therefore, considering the high affinity of Cr and Mo with boron, the mechanism of M_5B_3 boride precipitation in γ/γ′ eutectic might be explained by creep deformation facilitation. The high density of dislocations with Cr and Mo segregation in γ/γ′ eutectic provide sites for precipitation of M_5B_3 phase at high temperatures during the creep. And elements enriched in γ/γ′ eutectic region provide the source of elements for the formation of M_5B_3 phase. It is worth noting that other types of borides were not found in γ/γ′ eutectic of our alloy. This is possibly because of the low interfacial energy between M_5B_3 phase and γ/γ′ eutectic. Based on the diffraction analyses, the lattice parameter *c* for M_5B_3 phase is just three times that of γ/γ′ eutectic. Although M_3B_2 and M_5B_3 phase have the same lattice parameter *a* and very similar composition, the *c* for M_3B_2 phase is about 0.30 nm [33,34], which will result in higher interfacial energy between M_3B_2 and γ/γ′ eutectic.

The insufficient compatible deformation capability of γ/γ′ eutectic could result in high dislocation density in eutectic γ′ and at eutectic/matrix interfaces as reported by Wang et al. [35]. As shown in Fig. 5(a) and (b), high density of M_5B_3 particles formed in the γ channel, and the dislocation density is extremely high along the interface between eutectics and matrix. In addition, many stacking faults (marked by white arrows) were observed in the γ/γ′ eutectic. However, the dislocation density is still very low in the matrix far away from the γ/γ′ eutectic (see Fig. 5(c)). It is indicated that stress concentration could take place surrounding γ/γ′ eutectics. As reported by Yuan et al. [36], creep cracks can initiate at eutectic/matrix interfaces at high temperatures. Similarly, as can be seen from Fig. 5(d), the cracks at γ/γ′ eutectic/matrix interface were observed in our work. Thus, we suggest that the precipitation of nanosized granular borides at γ/γ′ eutectic regions is possible to deteriorate the plastic deformability of γ/γ′ eutectics. The nanosized M_5B_3 particles precipitate in matrix and distribute uniformly, which can hind the migration of γ/γ′ interface and be beneficial for creep properties. However. a large amount of nanosized M_5B_3 phase precipitated in the extremely narrow γ channel of γ/γ′ eutectics rather than matrix can further fix the dislocations, complicate the stress concentration surrounding γ/γ′ eutectics and aggravate the deformation incompatibility.

4. Conclusions

The present work has investigated the microstructure of γ/γ′ eutectic in a Ni-based superalloy before and after the creep. Though the boron usually segregates to grain boundaries, creep induced precipitation of M_5B_3 in γ/γ′ eutectic was observed in our case. The M_5B_3

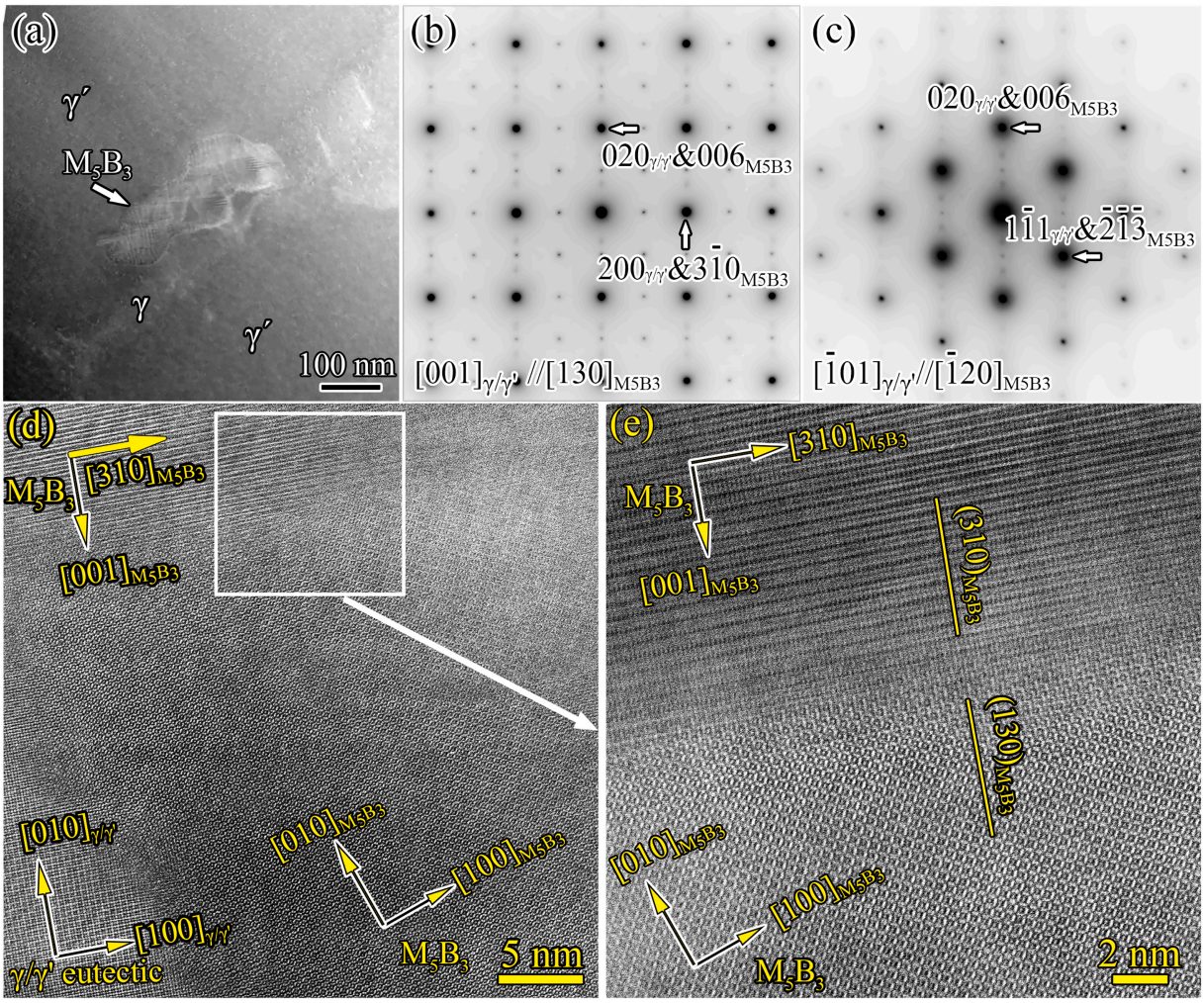

Fig. 2. A HAADF image of the region containing M_5B_3-type boride along the $[001]_{\gamma/\gamma'}$ direction (a); the inverted SAED patterns along $[001]_{\gamma/\gamma'}$ (b) and $[\bar{1}01]_{\gamma/\gamma'}$ (c) direction, respectively. HAADF images (d) and (e) showing intergrowth of M_5B_3 phases with different crystal orientations.

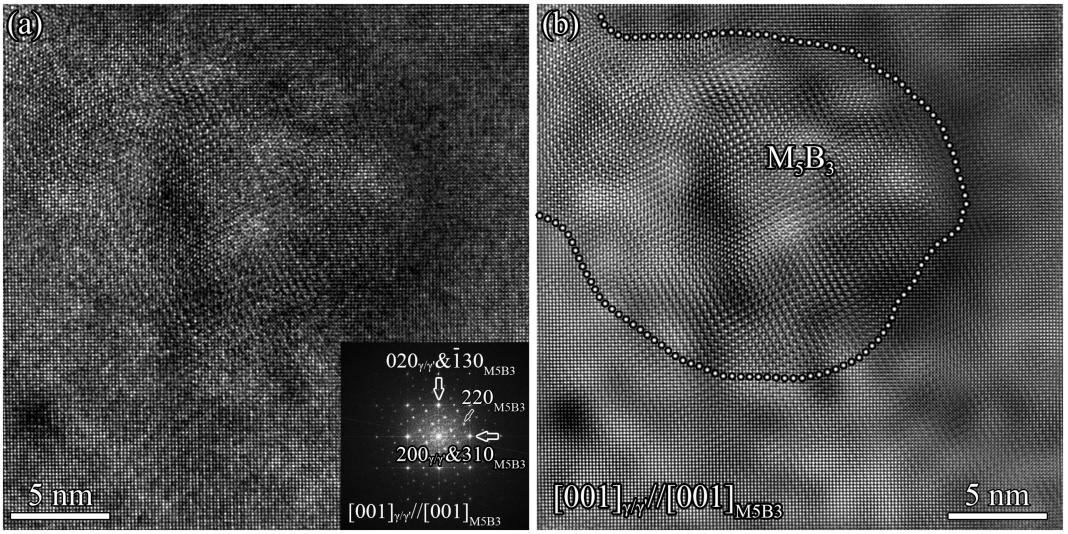

Fig. 3. HRTEM images showing the M_5B_3 boride about 15 nm in size, (a) the original image and (b) image processed by Fourier mask filtering (the M_5B_3 roughly marked with a dashed line). Inset in the bottom-right of (a) corresponds to FFT pattern.

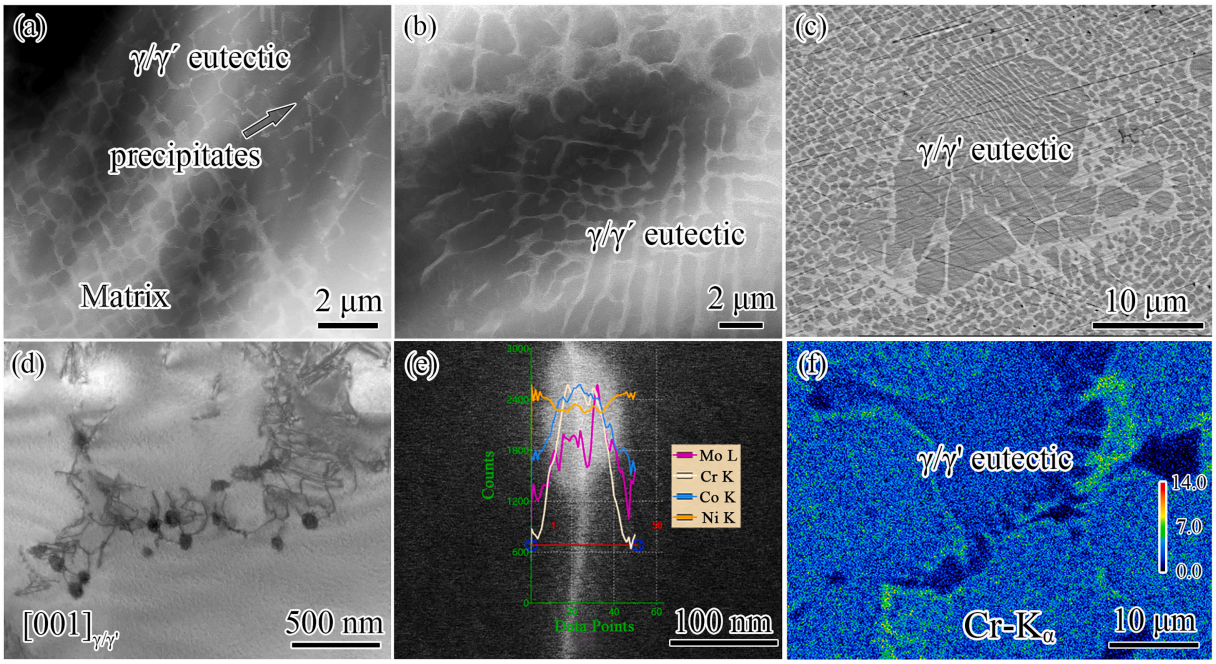

Fig. 4. HAADF images showing granular nanosized precipitates located at γ/γ′ eutectic region of the crept specimen (a), and no M_5B_3 phase particle precipitation were displayed in γ/γ′ eutectic of the as-cast specimen (b), respectively. (c) A BSE image showing no obvious precipitation in γ/γ′ eutectic compared to the crept specimen. (d) A BF image displaying granular precipitates linked by dislocations and (e) EDS line-scan profiles scanned across the dislocation showing the segregation of Cr, Mo and Co. (f) EPMA elemental mapping showing the Cr-rich crown of γ/γ′ eutectic in as-cast specimens.

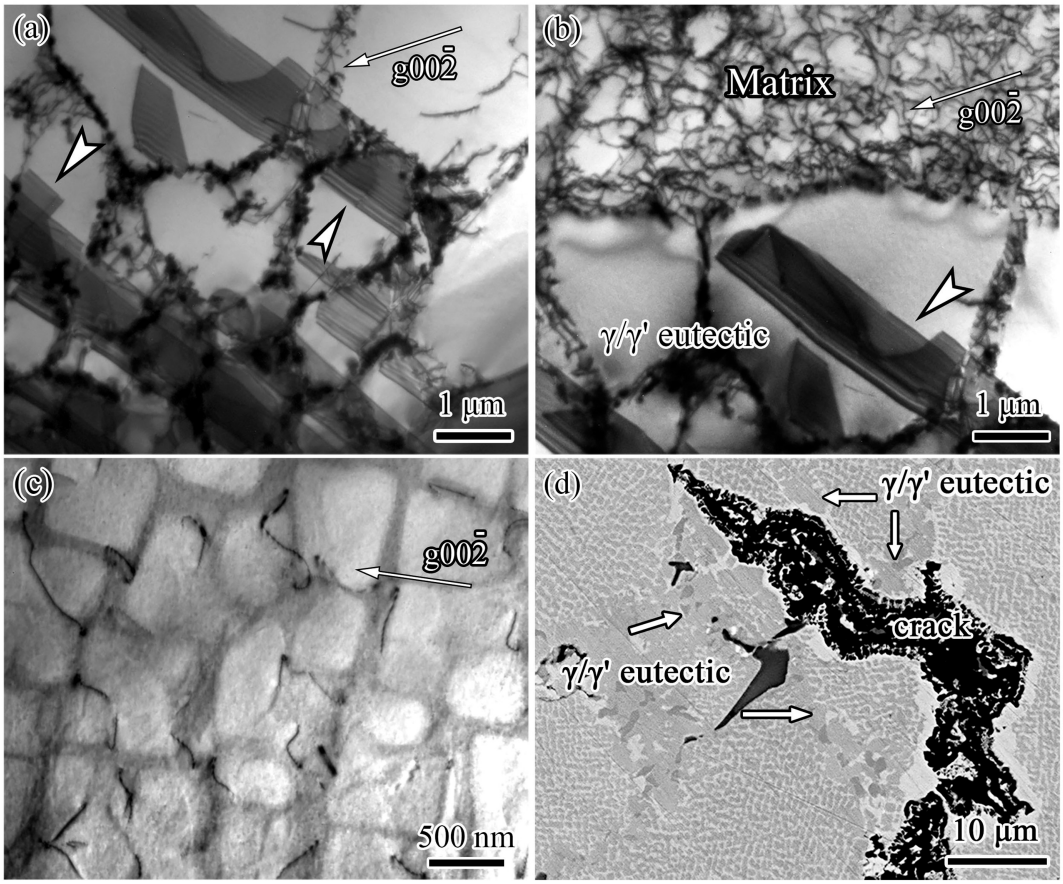

Fig. 5. BF-TEM images showing the configuration of stacking faults and dislocations in (a) γ/γ′ eutectic regions and (b) along the interface between matrix and eutectics in crept specimen. (c) The matrix with a small amount of dislocations far away from the γ/γ′ eutectic. (d) SEM image displaying creep cracks at γ/γ′ eutectic/matrix in BSE imaging mode.

exhibits a fixed orientation relationship with the γ/γ′ eutectic, which is $[001]_{\gamma/\gamma'}//[001]_{M5B3}$, $(020)_{\gamma/\gamma'}//(130)_{M5B3}$. Furthermore, this precipitation behavior can be explained as high density of dislocations confined within γ channel of eutectics provide driving force for M_5B_3 boride nucleation at elevated temperature. This study is helpful to understand the influence mechanism of boron on the high temperature creep properties of Ni-based superalloys.

Data availability

The raw/processed data will be provided as request.

Declaration of competing interest

The authors declare that they have no known competing financial interests or personal relationships that could have appeared to influence the work reported in this paper.

Acknowledgement

This work is supported by the National Natural Science Foundation of China (No. 51771201) and Joint Research Fund Liaoning-Shenyang National Laboratory for Materials Science (No. 20180510059). Many thanks to Mr. Bo Wu and Mr. Lixin Yang for transmission electron microscope technical support.

Appendix A. Supplementary data

Supplementary data to this article can be found online at https://doi.org/10.1016/j.matchar.2020.110569.

References

[1] R.C. Reed, The Superalloys: Fundamentals and Applications, Cambridge University Press, New York, 2008.
[2] D. Shifler, N.M. Division, Future research directions to understanding factors influencing advanced high temperature materials, 2009 DoD Corros. Conf. 2009.
[3] H.L. Ge, J.D. Liu, S.J. Zheng, Y.T. Zhou, Q.Q. Jin, X.H. Shao, B. Zhang, Y.Z. Zhou, X.L. Ma, Boride-induced dislocation channeling in a single crystal Ni-based superalloy, Mater. Lett. 235 (2019) 232–235, https://doi.org/10.1016/j.matlet.2018.10.039.
[4] B. Yin, G. Xie, L. Lou, J. Zhang, Abnormal increase of TCP phase during heat treatment in a Ni-based single crystal superalloy, Scr. Mater. 173 (2019) 1–4, https://doi.org/10.1016/j.scriptamat.2019.07.027.
[5] W. Zhang, P.K. Liaw, Y. Zhang, Science and technology in high-entropy alloys, Sci. China Mater. 61 (2018) 2–22, https://doi.org/10.1007/s40843-017-9195-8.
[6] B. Gedde, H. Leon, X. Huang, Superalloys: Alloying and Performance, ASM International, Ohio, 2010, https://doi.org/10.1016/B978-0-7020-2797-0.00001-1.
[7] P.J. Zhou, J.J. Yu, X.F. Sun, H.R. Guan, Z.Q. Hu, The role of boron on a conventional nickel-based superalloy, Mater. Sci. Eng. A 491 (2008) 159–163, https://doi.org/10.1016/j.msea.2008.02.019.
[8] B.C. Yan, J. Zhang, L.H. Lou, Effect of boron additions on the microstructure and transverse properties of a directionally solidified superalloy, Mater. Sci. Eng. A 474 (2008) 39–47, https://doi.org/10.1016/j.msea.2007.05.082.
[9] L. Xiao, D.L. Chen, M.C. Chaturvedi, Effect of boron and carbon on thermo-mechanical fatigue of IN 718 superalloy - part I. Deformation behavior, Mater. Sci. Eng. A 437 (2006) 157–171, https://doi.org/10.1016/j.msea.2006.05.130.
[10] D. Mukherji, J. Rösler, M. Krüger, M. Heilmaier, M.C. Bölitz, R. Völkl, U. Glatzel, L. Szentmiklósi, The effects of boron addition on the microstructure and mechanical properties of Co-Re-based high-temperature alloys, Scr. Mater. 66 (2012) 60–63, https://doi.org/10.1016/j.scriptamat.2011.10.007.
[11] H.J. Kim, Z. En, J.H. Ho, J.S. Jang, N. Jurneav, M.M. Usmanova, Boron distribution measurement in metals by neutron induced radiography, J. Radioanal. Nucl. Chem. 216 (1997) 117–120, https://doi.org/10.1007/BF02034506.
[12] E. Cadel, D. Lemarchand, S. Chambreland, D. Blavette, Atom probe tomography investigation of the microstructure of superalloys N18, Acta Mater. 50 (2002) 957–966, https://doi.org/10.1016/S1359-6454(01)00395-0.
[13] P. Kontis, H.A.M. Yusof, S. Pedrazzini, M. Danaie, K.L. Moore, P.A.J. Bagot, M.P. Moody, C.R.M. Grovenor, R.C. Reed, On the effect of boron on grain boundary character in a new polycrystalline superalloy, Acta Mater. 103 (2016) 688–699, https://doi.org/10.1016/j.actamat.2015.10.006.
[14] P. Kontis, E. Alabort, D. Barba, D.M. Collins, A.J. Wilkinson, R.C. Reed, On the role of boron on improving ductility in a new polycrystalline superalloy, Acta Mater. 124 (2017) 489–500, https://doi.org/10.1016/j.actamat.2016.11.009.
[15] Y. Zhao, C. Liu, Y. Guo, Y. Liu, J. Zhang, Y. Luo, D. Tang, Influence of minor boron on the microstructures of a second generation Ni-based single crystal superalloy, Prog. Nat. Sci. Mater. Int. 28 (2018) 483–488, https://doi.org/10.1016/j.pnsc.2018.06.001.
[16] Y.S. Zhao, J. Zhang, Y.S. Luo, J. Li, D.Z. Tang, Effects of Hf and B on high temperature low stress creep behavior of a second generation Ni-based single crystal superalloy DD11, Mater. Sci. Eng. A 672 (2016) 143–152, https://doi.org/10.1016/j.msea.2016.06.079.
[17] W.S. Walston, I.M. Bernstein, A.W. Thompson, The role of the γ/γ′ eutectic and porosity on the tensile behavior of a single-crystal nickel-base superalloy, Metall. Trans. A. 22 (1991) 1443–1451, https://doi.org/10.1007/BF02660676.
[18] X. Xia, Y. Peng, J. Zhang, X. He, S. Yin, J. Ding, C. Li, X. Chen, Y. Liu, Precipitation and growth behavior of γ′ phase in Ni_3Al-based superalloy under thermal exposure, J. Mater. Sci. 54 (2019) 13368–13377, https://doi.org/10.1007/s10853-019-03821-0.
[19] B. Ruttert, C. Meid, L. Mujica Roncery, I. Lopez-Galilea, M. Bartsch, W. Theisen, Effect of porosity and eutectics on the high-temperature low-cycle fatigue performance of a nickel-base single-crystal superalloy, Scr. Mater. 155 (2018) 139–143, https://doi.org/10.1016/j.scriptamat.2018.06.036.
[20] F. Wang, W. Xu, D. Ma, A. Bührig-Polaczek, Co-growing mechanism of γ/γ′ eutectic on MC-type carbide in Ni-based single crystal superalloys, J. Alloys Compd. 792 (2019) 505–509, https://doi.org/10.1016/j.jallcom.2019.04.067.
[21] B. Zhang, Y. Tong, J. Zhang, Z. Liu, Y. Zhu, Microstructure and solidication characteristics of M91 cast Ni-based superalloy, Acta Metall. Sin. 26 (1990) A438–A442.
[22] X.F. Yuan, W.R. An, Y.W. Ju, S. Antonov, Z.N. Bi, W. Li, J.T. Wu, Evaluation of microstructural degradation and its corresponding creep property in integral cast turbine rotor made of K424 alloy, Mater. Charact. 158 (2019), https://doi.org/10.1016/j.matchar.2019.109946.
[23] H.R. Zhang, O.A. Ojo, M.C. Chaturvedi, Nanosize boride particles in heat-treated nickel base superalloys, Scr. Mater. 58 (2008) 167–170, https://doi.org/10.1016/j.scriptamat.2007.09.049.
[24] P. Kontis, A. Kostka, D. Raabe, B. Gault, Influence of composition and precipitation evolution on damage at grain boundaries in a crept polycrystalline Ni-based superalloy, Acta Mater. 166 (2019) 158–167, https://doi.org/10.1016/j.actamat.2018.12.039.
[25] GB/T 2039-2012, Metallic materials—uniaxial creep testing in tension, China Standard Press (2012).
[26] B. Du, Z. Shi, J. Yang, Z. Chu, C. Cui, X. Sun, L. Sheng, Y. Zheng, M_5B_3 boride at the grain boundary of a nickel-based superalloy, J. Mater. Sci. Technol. 32 (2016) 265–270, https://doi.org/10.1016/j.jmst.2015.11.010.
[27] D.B. Williams, C.B. Carter, Transmission electron microscopy: a textbook for materials science, Springer, US Boston, 2009.
[28] X.B. Hu, L.Z. Zhou, J.S. Hou, X.Z. Qin, X.L. Ma, Interfacial precipitation of the M_5B_3-type boride in Ni-based superalloys, Philos. Mag. Lett. 96 (2016) 273–279, https://doi.org/10.1080/09500839.2016.1200756.
[29] M. Huang, Z. Cheng, J. Xiong, J. Li, J. Hu, Z. Liu, J. Zhu, Coupling between Re segregation and γ/γ′ interfacial dislocations during high-temperature, low-stress creep of a nickel-based single-crystal superalloy, Acta Mater. 76 (2014) 294–305, https://doi.org/10.1016/j.actamat.2014.05.033.
[30] T.M. Smith, B.D. Esser, N. Antolin, G.B. Viswanathan, T. Hanlon, A. Wessman, D. Mourer, W. Windl, D.W. McComb, M.J. Mills, Segregation and η phase formation along stacking faults during creep at intermediate temperatures in a Ni-based superalloy, Acta Mater. 100 (2015) 19–31, https://doi.org/10.1016/j.actamat.2015.08.053.
[31] B. Zhang, G. Sheng, Y. Jiao, Z. Gao, X. Gong, H. Fan, J. Zhong, Precipitation and evolution of boride in diffusion affected zone of TLP joint of Mar-M247 superalloy, J. Alloys Compd. 695 (2017) 3202–3210, https://doi.org/10.1016/j.jallcom.2016.11.306.
[32] H.W. Zhang, Y.S. Wu, X.Z. Qin, L.Z. Zhou, X.W. Li, Microstructures and high-temperature mechanical properties of a directionally solidified Ni-based superalloy: influence of boron content, J. Alloys Compd. 767 (2018) 915–923, https://doi.org/10.1016/j.jallcom.2018.07.162.
[33] N. Sheng, X. Hu, J. Liu, T. Jin, X. Sun, Z. Hu, M_3B_2 and M_5B_3 formation in diffusion-affected zone during transient liquid phase bonding single-crystal superalloys, Metall. Mater. Trans. A 46 (2015) 1670–1677, https://doi.org/10.1007/s11661-014-2733-z.
[34] X.B. Hu, H.Y. Niu, X.L. Ma, A.R. Oganov, C.A.J. Fisher, N.C. Sheng, J.D. Liu, T. Jin, X.F. Sun, J.F. Liu, Y. Ikuhara, Atomic-scale observation and analysis of chemical ordering in M_3B_2 and M_5B_3 borides, Acta Mater. 149 (2018) 274–284, https://doi.org/10.1016/j.actamat.2018.02.055.
[35] L. Wang, F. Pyczak, J. Zhang, L.H. Lou, R.F. Singer, Effect of eutectics on plastic deformation and subsequent recrystallization in the single crystal nickel base superalloy CMSX-4, Mater. Sci. Eng. A 532 (2012) 487–492, https://doi.org/10.1016/j.msea.2011.11.015.
[36] X.F. Yuan, J.T. Wu, J.T. Li, W. Li, J.C. Zhao, P. Yan, Effects of initial microstructures on the microstructural evolution and corresponding mechanical property of K424 superalloy after overheating exposure, Mater. Sci. Eng. A 743 (2019) 40–56, https://doi.org/10.1016/j.msea.2018.11.027.